

# Highly sensitive crumpled 2D material-based plasmonic biosensors

VAHID FARAMARZI, 1 D VAHID AHMADI, 1,\* D MICHAEL T. HWANG, 2 AND PETER SNAPP<sup>3</sup>

**Abstract:** We propose surface plasmon resonance biosensors based on crumpled graphene and molybdenum disulphide (MoS<sub>2</sub>) flakes supported on stretchable polydimethylsiloxane (PDMS) or silicon substrates. Accumulation of specific biomarkers resulting in measurable shifts in the resonance wavelength of the plasmon modes of two-dimensional (2D) material structures, with crumpled structures demonstrating large refractive index shifts. Using theoretical calculations based on the semiclassical Drude model, combined with the finite element method, we demonstrate that the interaction between the surface plasmons of crumpled graphene/MoS<sub>2</sub> layers and the surrounding analyte results in high sensitivity to biomarker driven refractive index shifts, up to 7499 nm/RIU for structures supported on silicon substrates. We can achieve a high figure of merit (FOM), defined as the ratio of the refractive index sensitivity to the full width at half maximum of the resonant peak, of approximately 62.5 RIU<sup>-1</sup>. Furthermore, the sensing properties of the device can be tuned by varying crumple period and aspect ratio through simple stretching and integrating material interlayers. By stacking multiple 2D materials in heterostructures supported on the PDMS layer, we produced hybrid plasmon resonances detuned from the PDMS absorbance region allowing higher sensitivity and FOM compared to pure crumpled graphene structures on the PDMS substrates. The high sensitivity and broad mechanical tunability of these crumpled 2D material biosensors considerable advantages over traditional refractive index sensors, providing a new platform for ultrasensitive biosensing.

© 2021 Optical Society of America under the terms of the OSA Open Access Publishing Agreement

#### Introduction

Surface plasmon polaritons (SPPs) are collective oscillations of free electrons propagating at the interface between a dielectric and a conductor. As SPPs confine the optical energy of light into the subwavelength scale [1] they play an important role in biosensors [2], filters [3], lasers [4], logic gates [5], and modulators [6]. Furthermore, as surface plasmon modes are sensitive to environmental parameters even slight changes in the refractive index of the sensing medium can dramatically affect the characteristics of the SPP modes including resonance wavelength. As a result surface plasmon resonance (SPR)-based biosensors have attracted intensive attention as biomedical diagnostic and food safety monitoring devices [7–9], enabled by their compact structure and high sensitivity [10,11], achieving real-time detection of [12]. Traditional SPR-based sensors are based on noble metals such as silver and gold due to their high electrical conductivity and wide plasma frequencies in the ultraviolet and visible frequency regions. However, the vibrational fingerprints of biomolecule building blocks, such as proteins and DNA are lie in the mid-IR range, which is exclusively desired for biosensing [13,14]. One of the key approaches to biosensing is the detection of changes in the refractive index of the medium around the sensor

#428537 https://doi.org/10.1364/BOE.428537 Journal © 2021 Received 22 Apr 2021; revised 17 Jun 2021; accepted 18 Jun 2021; published 29 Jun 2021

 $<sup>^{</sup>m \it l}$  Department of Electrical and Computer Engineering, Tarbiat Modares University, 14115-194, Tehran,

<sup>&</sup>lt;sup>2</sup>Department of BioNano Technology, Gachon University, 1342 Seongnamdae-ro, Sujeong-gu, Seongnam, Gyeonggi, 13120, Republic of Korea

<sup>&</sup>lt;sup>3</sup>Department of Mechanical Science and Engineering, University of Illinois at Urbana-Champaign, IL 61801, USA

v\_ahmadi@modares.ac.ir

surface driven by the accumulation of biochemical species in the vicinity of the sensor surface, allowing for real time biosensing. Because of the significant mismatch between the micrometer scale IR wavelengths and nanometer scale size of biomolecules, the light-molecule interaction is insufficient and IR absorption signals are extremely weak. The optical near-field penetration within the metal in the IR range is weak as compared with UV-visible frequencies [15–17]. Thus, due to weak optical field confinement into the metal surface, a device with a larger dimension is required therefore, device integration becomes challenging [18]. Furthermore, metals, such as gold, present high losses at infrared frequencies, have very limited tunability [19] and do not adsorb biomolecules perfectly due to their intrinsic hydrophobicity motivating exploration of emergent two dimensional (2D) materials as platforms for SPR phenomena [20].

In contrast, graphene, a single atomic layer of carbon atoms with high electron mobility, electrical/thermal conductivity, and flexibility [21,22], has been demonstrated to support plasmons in mid-infrared and far-infrared ranges with high spatial electromagnetic field confinement and low dissipation loss. Furthermore, graphene plasmon resonances can be tuned through chemical doping or electrostatic gating into the infrared and terahertz regions [23]. Monolayer molybdenum disulphide (MoS<sub>2</sub>) is also a promising plasmonic material, which shows high near-field confinement, localization, and low losses in the mid-infrared [24]. The high field confinement of the 2D materials plasmons increases interaction with nanoscale biomolecules, increasing sensitivity when monitoring biomolecule driven changes in analyte refractive index.

Unfortunately, coupling between surface plasmons and free-space electromagnetic waves, due to a large mismatch between the plasmon and incident light wave vectors. is still a challenge preventing the realization of plasmonic devices based on 2D materials, Furthermore conventional optical coupling configurations including prism couplers [25], grating couplers [26], and waveguide couplers [27] are bulky and difficult to fabricate [28]. Similarly, while plasmonic resonances can be simply excited in patterned graphene sensors, patterned configurations are difficult to fabricate, are not reconfigurable [29,30], and present challenges in realizing broadband tunable graphene plasmons [31]. It is possible to sidestep the issue of patterning 2D materials by using textured graphene which has been deformed to produce periodic structures using macroscale compressive strain. and can form the basis for mechanically reconfigurable plasmonic structures to support plasmon resonances with broadband tunability [32]. Recent studies have shown that crumpled graphene structures can be fabricated on different thermally or mechanically flexible and stretchable substrates [33,34]. After transferring graphene onto an underlying thermally activated polymer substrate such as polystyrene film or pre-stretched elastomer substrate such as polydimethylsiloxane (PDMS) [35], graphene is forced into a textured configuration during substrate shrinkage due to heating or release of strain. This induced structure enables strong coupling between free space electromagnetic waves which can be tuned by subsequent application of strain to modify crumple structure. It has been recently demonstrated that crumpled graphene field effect transistors (gFETs) present superior sensitivity in biomolecule detection compared to the flat gFET [36,37]. In addition, wrinkled graphene structures have been utilized to improve surface-enhanced Raman spectroscopy (SERS) substrate [38].

In this work, we report, for the first time, the use of reconfigurable crumpled pure 2D material and 2D materials heterostructure plasmonic structures as plasmonic biosensors. We investigate how the plasmonic resonance wavelength of a crumpled 2D material sensor shifts in response to variations in the refractive index of an analyte solution using theoretical calculations based on the semiclassical Drude model, combined with the finite element method. Changes in biomolecule concentration in the solution induce a local change in the refractive index shifting the propagation constant of plasmonic waves, eventually leading to measurable red-shifts in the resonant wavelength of surface plasmons. The high sensitivity of 2D material plasmon modes to small changes in the optical properties of the surrounding medium allows detection of extremely small changes in the refractive index of the neighboring samples. The performance of

the proposed structures is evaluated in terms of sensor resonant wavelength shift over the change in refractive index and figure of merit (FOM) [39] defined as the ratio of the refractive index shift sensitivity to the full width at half maximum of the resonant peak, which quantifies the sharpness of the shifting resonant peak and therefore the minimum resolution for monitoring refractive index change. We show that the shift in plasmonic resonance wavelength for a given change in refractive index and the corresponding FOM for textured graphene is larger than that achieved by conventional, flat graphene-based plasmonic devices. Furthermore, we explore a hybrid plasmonic resonance with high electric field confinement and localization observed in heterogenous crumpled graphene/MoS<sub>2</sub> structures in the mid-infrared region. By stacking a crumpled MoS<sub>2</sub> atop the graphene flake new resonance peaks emerge due to plasmon hybridization within the spacing between the 2D material films. These emergent hybrid plasmons possess lower FWHM and higher absorption intensity, compared to the plasmon resonances of crumpled structures composed solely of graphene or MoS<sub>2</sub>. Furthermore, these resonances are readily tuned by controlling the crumpled structure parameters including the crumple height and period. Finally, the optical response spectra of the proposed heterostructure can be tuned by altering the Fermi level in graphene and carrier concentration in MoS2 flake allowing even more sophisticated tuning of sensitivity. These observations indicate the crumpled MoS<sub>2</sub>-graphene heterostructure is a promising platform for developing highly tunable and ultrasensitive plasmonic biosensors. The superiority of the proposed structures is comprehensively investigated in terms of sensitivity, FOM, and quality factor (Q). Our results indicate that crumpled pure 2D material and mixed 2D material heterostructures structures can be used as a new reconfigurable plasmonic biosensor with broadband tunability across the infrared range of light.

#### 2. Method

We performed full-wave optical simulations using COMSOL Multiphysics based on the finite element method (FEM) to investigate the absorption spectra (far-field response) of crumpled two-dimensional (2D) materials structures, and radio frequency module with periodic boundary condition is used. It has been shown that 2D surface conductivity model is useful and efficient in the simulation of graphene-based devices [40]. In our numerical simulations, the graphene layer is modeled as a thin film with a thickness (t) of 0.34 nm and 2D surface conductivity ( $\sigma_{Gr}$ ). Since the photon energy is less than  $2E_f$  in mid-infrared frequency region, the interband transition effect is neglected and the intraband conductivity of graphene at mid-infrared frequencies can be characterized with a semiclassical Drude model [41] as

$$\sigma_{Gr}(\omega) = (2e^2)/(\pi\hbar^2)k_BT_k \times ln[2 \times cosh(E_f/(2k_BT_k))]i/(\omega + i\tau_{Gr}^{-1})$$
 (1)

where  $T_k$  is the temperature,  $k_B$  is the Boltzmann constant,  $\hbar$  is the reduced Planck constant,  $\tau_{Gr}$  is the carrier relaxation time which determines the carrier mobility  $\mu$  in graphene as  $\tau_{Gr} = \mu E_f/ev_f^2$ , and  $E_f = \hbar v_f (\pi n)^{-1/2}$  is the Fermi energy level, where  $v_f = 10^6$  m/s is the Fermi velocity and n is the carrier density in graphene. In the simulations, the graphene layer is modeled as boundaries using transition boundary condition with an anisotropic dielectric function described by a diagonal tensor. The in-plane permittivity tensor components are  $\varepsilon_{r_{11}} = \varepsilon_{r_{22}} = 2.5 + i\sigma_{Gr}/(\varepsilon_0\omega t)$ , and the normal component to the surface is defined as  $\varepsilon_{r_{33}} = 2.5$  based on the graphite permittivity. The MoS<sub>2</sub> layer can be treated as a thin film material like graphene with a thickness of 0.68 nm.

In the mid-infrared region, the interband transition can be ignored and the intraband contribution to the conductivity dominates the light- $MoS_2$  interaction [42]. We describe the 2D conductivity of n-doped  $MoS_2$  by the Drude model,

$$\sigma(\omega) = \frac{n_{2D}e^2}{m^*} \frac{i}{\omega + i\tau_{MoS}^{-1}}$$
 (2)

where  $n_{2D}$  denotes the charge carrier concentration of MoS<sub>2</sub>,  $\tau_{MoS_2}$  is the carrier relaxation time, and  $m^*$  is the electron effective mass. In the modeling of MoS<sub>2</sub> layer, we use the values  $\tau_{MoS_2} = 0.17$  ps and  $m^* = 0.53m_e$ , where  $m_e$  is the electron mass.

The use of crumpled structures can compensate for the wave vector mismatching between the free-space electromagnetic wave and plasmon. The crumpled structure is formed by releasing a pre-strained stretchable substrate such as PDMS after the graphene or MoS<sub>2</sub> transferring process. Under normal-incidence conditions and optical energy dissipation due to Ohmic loss in 2D materials, a sharp resonance peak can be seen in the absorption spectrum around the resonant frequency. To model the sensor used for biosensing, the sensing medium to be detected is placed on top of the structure surface. For undulated structures the wrinkles are filled by substrate material, however, for flat substrates, the region between the apex of the crumpled 2D material and substrate is filled by air with a refractive index of 1. The refractive index range of the sensing medium was selected to cover commonly used biomolecules such as human serum albumin, single-stranded DNA, and double-stranded DNA.

A periodic port is chosen in the z-direction in order to illuminate the structure and periodic boundary condition is applied to the unit cell on the respective crumpling directions to simulate the real structure with an array of infinite unit cells. A transverse electric field propagating along the crumpling direction is radiated in the normal direction to the structure. During simulation, non-uniform mesh sizes are used to decrease the simulation time and memory. The accuracy of mesh for 2D materials boundaries along the x axis is set to 0.1 nm and mesh sizes increase gradually outside the 2D materials layers with a mesh growth rate of 1.25. To ensure the accuracy of the calculations in the mesh generation process, simulations are performed until convergence is achieved. The minimum mesh size of 0.1 nm is assigned to the 2D materials boundaries and extremely refined mesh size is used in other regions. In the simulations, the maximum mesh element size is 29 nm and a mid-infrared light source illuminates the structure from the top port. Scattering (S) parameters of the proposed device in this work are calculated using the finite element method [43]. The S parameters not only can be used to derive the effective refractive index of the plasmonic sensors but also are employed to determine optical responses (i.e., transmission, reflection, or absorption spectra), and resonance wavelengths of the 2D materials structures. The transmission and reflection coefficient spectra can be achieved by solving Maxwell equations and defined as  $T_i = |S_{21}|^2$  and  $R_i = |S_{11}|^2$ , respectively. Therefore, the absorption spectrum can be obtained as  $A_i = I - T_i - R_i$ . The heterostructure can be formed by stacking 2D materials on top of each other. Using the optical conductivity of 2D materials, the absorption spectrum of heterostructure is obtained by solving the Maxwell equations and matching the boundary conditions including the conductance and permittivity of the 2D materials

In the simulations, the refractive index of silicon and SiO<sub>2</sub> substrates in mid-infrared were taken from Kischkat [44]. The dielectric constants for PDMS substrate were taken from Zhang [45].

## 3. Results and discussions

We investigated the plasmonic resonances of the crumpled graphene,  $MoS_2$ , and graphene/ $MoS_2$  heterostructures placed on different substrates. The sensor is composed of a crumpled 2D material layer on a stretchable substrate (Fig. 1(a)). Crumpled graphene is assumed to adopt a sinusoidal shat with characteristic wavelength (T) and crumple height (H). Transverse magnetic (TM) polarized light along the crumpling direction x irradiates the system in the normal direction to the structure ( $k_0$ ). To observe the plasmonic resonances in the proposed crumpled graphene/ $MoS_2$  structure, we have studied the absorption spectrum for the proposed device at normal incidence with the E-field polarization along the x-axis in Fig. 1. The 2D material electrical properties are defined by the parameters in Table 1.

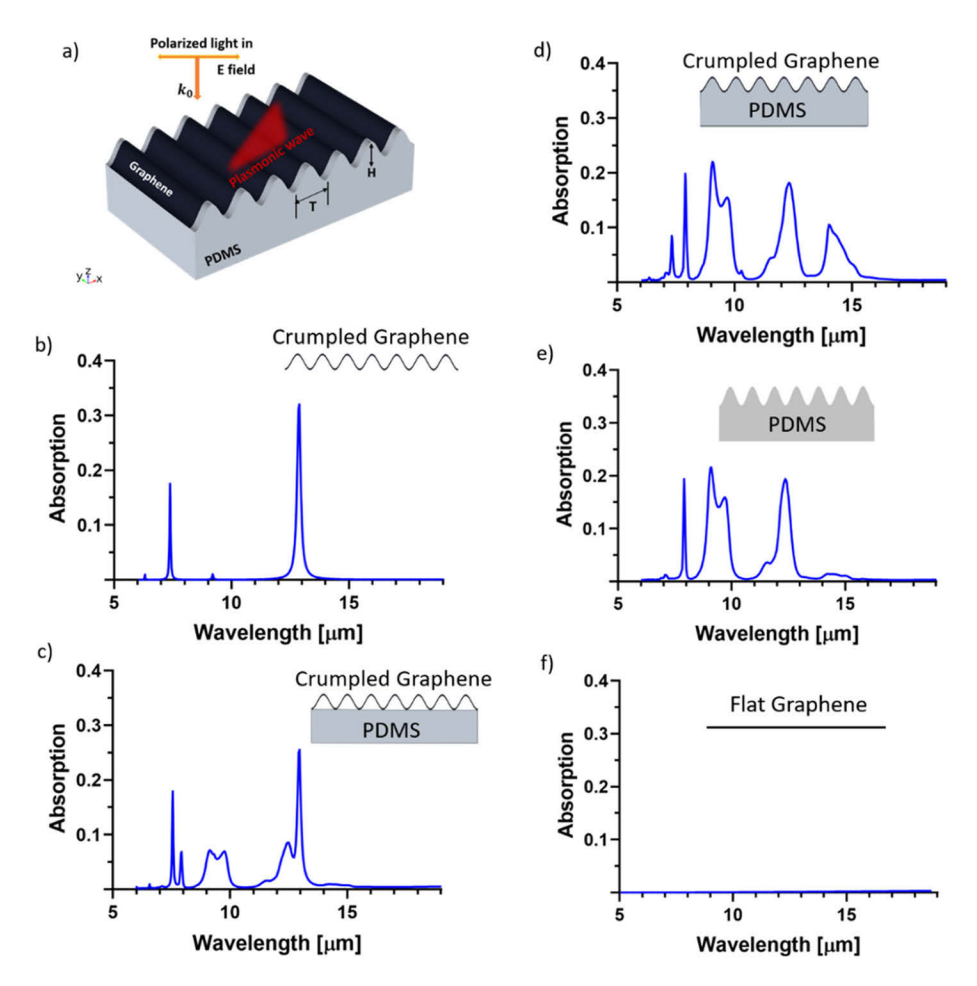


**Fig. 1.** The effect of PDMS substrate on the plasmonic resonance of crumpled graphene. (a) Schematic demonstration of a crumpled graphene structure with crumple period T and crumple height H. Polarized light with electric field E along the crumpling direction x illuminates in the normal direction  $k_0$  to the structure. (b) Optical absorption spectra of free-standing crumpled graphene, (c) crumpled graphene supported on flat PDMS substrate, (d) crumpled graphene placed on corrugated PDMS substrate, (e) bare corrugated PDMS structure, with  $T=150\,\mathrm{nm}$  and  $H=350\,\mathrm{nm}$ . Carrier mobility  $\mu$  and Fermi energy level  $E_F$  are adjusted to  $10000\,\mathrm{cm}^2/(\mathrm{V.s})$  and  $0.64\,\mathrm{eV}$ , respectively. (f) Absorption spectra of free-standing flat graphene as control. The insets indicate schematic demonstrations of the crumpled graphene without and with a substrate.

Table 1. Summary of the variable name, value, and definition of the electrical parameters of graphene and MoS<sub>2</sub> layers

| Definition                                  | Label         | Value    | Unit         |
|---|---------------|----------|--------------|
| Fermi velocity                              | $v_f$         | $10^{6}$ | m/s          |
| Carrier mobility of graphene                | $\mu$         | 10000    | $cm^2/(V.s)$ |
| Fermi energy level                          | $E_f$         | 0.64     | eV           |
| Carrier relaxation time of MoS <sub>2</sub> | $	au_{MoS_2}$ | 0.17     | ps           |
| Temperature                                 | $T_k$         | 300      | K            |

To establish the baseline plasmonic characteristics of devices composed of crumpled graphene we simulated flat and crumpled graphene on various substrates immersed in water No resonance peaks can be observed in the absorption spectrum of free-standing flat graphene (Fig. 1(f)). However, two absorbance peaks at the resonance wavelengths of  $\sim$ 7.3 and  $\sim$ 12.8  $\mu$ m, corresponding to the first and second resonance modes of the crumpled graphene suspended in water can be observed in Fig. 1(b), respectively.

To better model the performance of a physically realizable device we simulated the effect of a PDMS supporting layer on the plasmonic properties of crumpled graphene. Crumpled PDMS without graphene shows a sharp peak in absorption around 8 µm and broader spectral peaks at 9.2, 9.7, and 12.5 µm (Fig. 1(e)). For crumpled graphene supported on the flat PDMS substrate, we can clearly observe the plasmon resonance peaks similar to the free-standing crumpled graphene along with PDMS absorbance peaks. For the whole crumpled graphene-PDMS structure a wide peak can be seen at a wavelength of 14 µm in the absorption spectrum. This peak arises from the spectral overlap between the plasmon resonance of crumpled graphene and the wide absorbance spectral peak of PDMS substrate and results in damping and broadening of the plasmonic resonance. This obscuring of the graphene plasmonic resonance will make determination of subsequent shifts in the graphene plasmonic resonance difficult. Also, the intensity of the plasmon peak at  $\sim 7.3 \,\mu m$  decreases from 0.17 to 0.08, compared to the fee-standing crumpled graphene structure. With this confirmation that strong absorption peaks emerge in crumpled graphene as the result of plasmonic resonances which persist on different substrates, we proceed to explore how these plasmonic resonances are influenced by analyte solutions introduced into the crumpled graphene sensors environment.

We proceeded to examine how varying the refractive index of the medium  $(n_1)$  around the crumpled graphene, simulating the effect of an accumulating biomarker, affects the absorption spectra of the crumpled graphene. Figure 2 depicts the absorption spectra of the sensor shown in Fig. 1 as medium  $n_1$  varies from 1.3 to 1.5 around the surface of crumpled graphene. An obvious redshift in the resonance wavelength appears by increasing the refractive index surrounding the surface of the graphene layer. As can be observed in Fig. 2(a), as the refractive index of the medium increases from 1.3 to 1.5, the resonance wavelength of the main mode red-shifts from 12.88 µm to 14.85 µm, for bare crumpled graphene structure. The shifts for the main plasmon modes of the crumpled graphene on the flat PDMS and corrugated PDMS structures are 1942nm and 1252 nm, respectively. This reduction in wavelength shift of plasmon mode is attributed to the absorbance resonances and therefore damping effects of PDMS substrate in the mid-infrared region. The sensitivity of the sensor is defined as  $S_S = \Delta \lambda / \Delta n$  in nanometer per refractive index unit (nm/RIU), which identifies the rate of spectral shift in the resonance wavelength with respect to refractive index variations of the cover medium. The FOM as an effective parameter to evaluate the overall performance of the proposed sensor, is defined as  $FOM = S_S(nm.RIU^{-1})/\Delta\lambda(nm)$ , where  $S_S$  is the sensor sensitivity of the crumpled structure and  $\Delta \lambda$  is the resonance line width. In subsequent investigations of sensor sensitivity, we focus on the strongest plasmonic resonance mode. For the sensors designed by parameters given in Fig. 2, the overall sensor sensitivity is calculated as  $S_S = 9850$  nm/RIU for freestanding crumpled graphene without a substrate. The sensitivity for crumpled graphene on the flat PDMS and corrugated PDMS substrates is 9,710 and 6,260 nm/RIU, respectively. The amount of shift in the resonance wavelength, and thus the sensitivity of the sensor, can be further tuned by the mechanical reconfiguration of crumpled graphene structures.

We investigated plasmonic resonance wavelength shifts of crumpled graphene structures in the solutions with different refractive indices from 1.3 to 1.5 for various crumple heights and periods. We investigated the wavelength tunability of the plasmonic sensor by mechanical reconfiguration of crumpled graphene structures. We observed the optical absorption of crumpled graphene on PDMS substrate in Fig. 3 for different geometries, with varying crumple periods and heights,

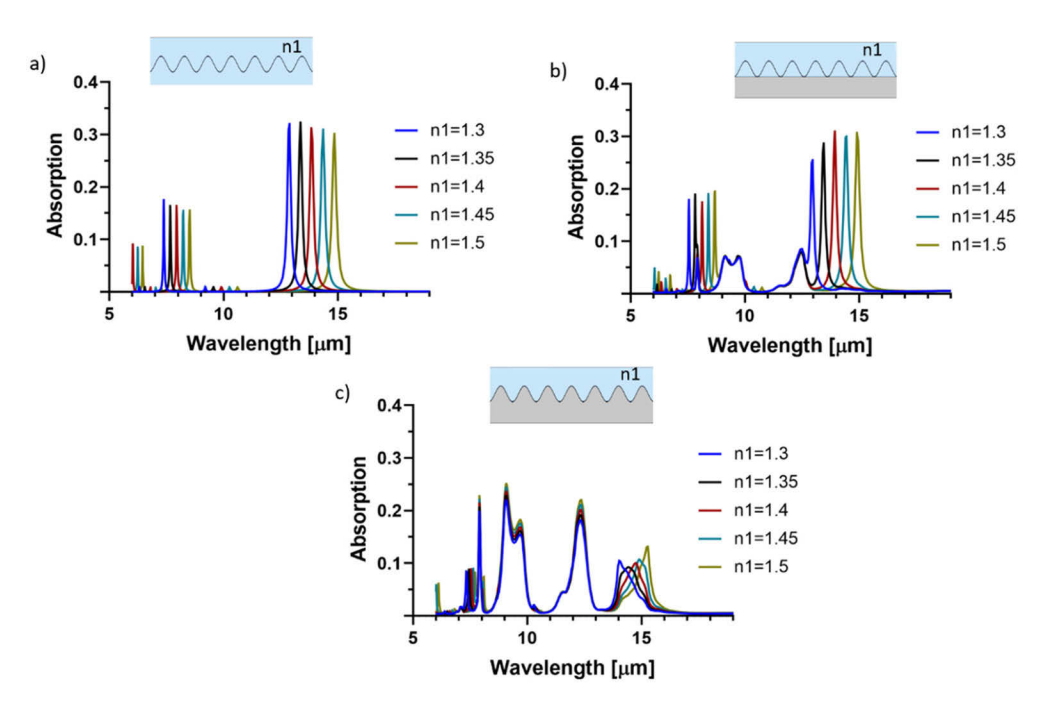


**Fig. 2.** Plasmonic resonance shifts of crumpled graphene structures for different refractive indices of sample medium. (a) Normal-incidence optical absorption spectra of free-standing crumpled graphene, (b) crumpled graphene supported on flat PDMS substrate, and (c) crumpled graphene placed on corrugated PDMS substrate when the refractive index of the sample  $n_1$  changes from 1.3 to 1.5 with geometrical parameters of T=150 nm and T=150 nm, and electronic properties of T=150 nm and T=150 nm, and electronic properties of the crumpled graphene without and with a substrate placed in a solution with refractive index n1.

when the refractive indices of medium atop the graphene layer ranges from 1.3 to 1.5. The sensor sensitivity varies between 1287 nm/RIU to 2376 nm/RIU for the structures shown in Fig. 3. No significant plasmonic resonance and its subsequent wavelength shift can be observed for the structures with high aspect ratios of crumple period to height (T/H) and small crumple features.

To potentially obtain a signal with more distinct resonant peaks and avoid the damping effects of the PDMS layer, we can transfer the crumpled graphene onto a commonly-used transparent substrate in the mid-infrared region such as silicon. This may be feasible by removing the PDMS layer within the etchant solution and transferring it onto the silicon substrate. In this regard, the crumpling parameters including crumple height and period can be adjusted by mechanical reconfiguration of the crumpled structure on the PDMS. Through the etching and removing the PDMS layer inside the etchant solution, the crumpled graphene can be suspended on the solution surface consequently can be transferred on the transparent mid-infrared silicon substrate. By transferring the periodic crumpled graphene structure on the silicon substrate, an air region can be created between the apex area of the crumpled graphene and flat silicon substrate. More plasmon resonances can be observed in the photo-absorption spectrum of crumpled graphene placed on the silicon substrate (Fig. 4(b)). Due to the strong damping effect of the PDMS layer, these plasmonic modes are greatly attenuated, therefore not appear in the absorption spectrum of crumpled graphene on the PDMS substrate. Figure 4, compares the sensitivity of the crumpled graphene structures with geometrical parameters of T = 250 nm and H = 300 nm on the PDMS and silicon substrates. For crumpled graphene on the silicon substrate, we investigated refractive

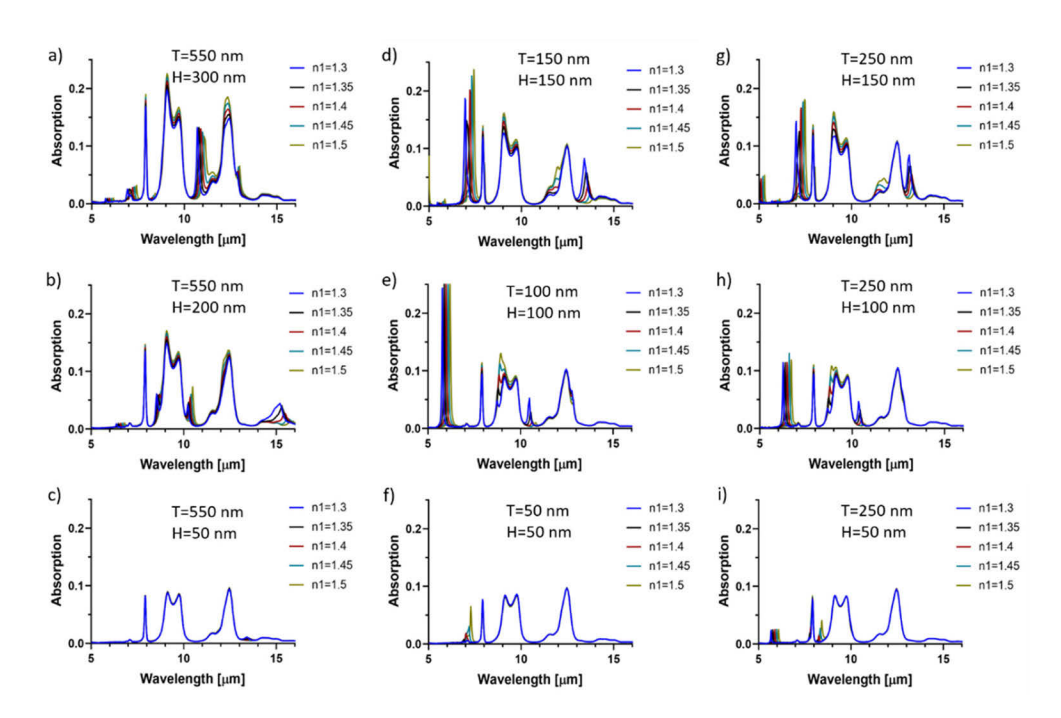


**Fig. 3.** Geometry dependence of the plasmonic resonance shifts in crumpled graphene structures. Normal-incidence optical absorption spectra of crumpled graphene supported on the PDMS substrate with varying H (= 50-300 nm) at T = 550 nm ((a), (b), and (c)), with varying T (= 50-150 nm) at T/H = 1 ((d), (e), and (f)), and with varying H (= 50-150 nm) at T = 250 nm ((g), (h), and (i)). The refractive index of sample  $n_1$  varies from 1.3 to 1.5. The electronic properties of graphene are set as  $E_F$  = 0.64 eV and  $\mu$  = 10000c m<sup>2</sup>/(V.s).

index changes on top of the graphene layer (Fig. 4(b)). As shown in Fig. 4, the sensitivity of the crumpled graphene structure to the refractive index versions atop the graphene layer supported on PDMS and silicon substrates is 2094nm/RIU and 7499 nm/RIU, respectively. Table 2 compares the sensing performance of the proposed crumpled graphene sensor with some graphene-based refractive index sensors studies, which have recently been published. The parameters in the last row are listed for the crumpled graphene sensor investigated in this paper. Our proposed sensor shows superior metrics regarding sensitivity, FOM compared with recently reported graphene-based sensors in the infrared region of light. Along with superior metrics, the broad spectral tunability of this flexible sensor is achieved by facile mechanical reconfiguration of crumpled structure.

In experiments, due to the point defects and impurities introduced during the graphene transfer process on the substrate the electron mobility in graphene is below  $10000~\text{cm}^2/(V.s)$ , while the mobility in a suspended exfoliated graphene can surpass  $230000~\text{cm}^2/(V.s)$ . More defects and residual impurity can be observed in graphene on the different substrates, which can decrease the electron mobility of the graphene layer. The lower mobility corresponds to higher propagation loss and lower quality factor (Q) of plasmonic resonances. The Q-factor is defined as  $\lambda_0$  / $\Delta\lambda$ , where  $\lambda_0$  and  $\Delta\lambda$  are resonance wavelength and FWHM of the plasmon resonance mode, respectively. Therefore, due to optical loss in graphene the resonance peaks in the absorption spectra become broader with lower intensity. This can affect the performance of the plasmonic biosensors in terms of sensitivity, FOM, and Q-factor. We study the effect of the optical loss on the performance of the plasmonic sensor by calculating absorption spectra of the crumpled graphene on silicon substrate when the electron mobility in the graphene layer varies from 10000

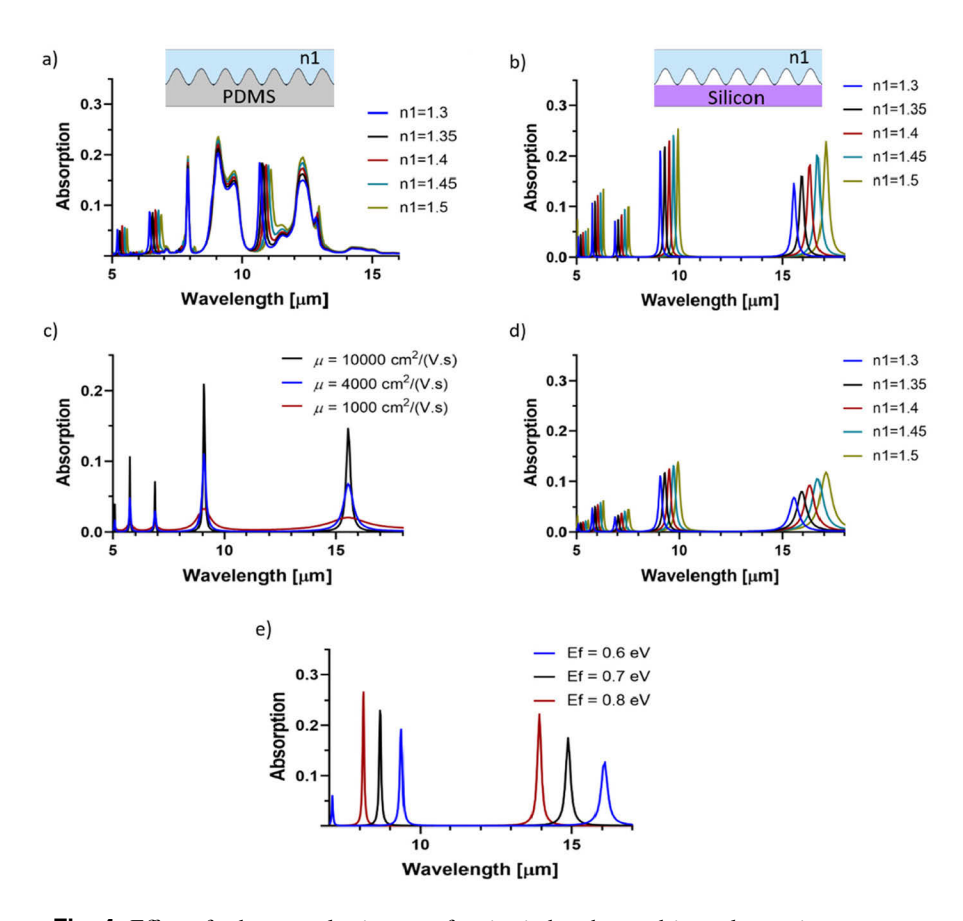


**Fig. 4.** Effect of substrate selection on refractive index change driven plasmonic resonance shifts in crumpled graphene structures. (a) Normal-incidence optical absorption spectra of crumpled graphene on corrugated PDMS substrate, (b) crumpled graphene surported on flat silicon substrate when the refractive index of solution atop the graphene surface  $n_1$  changes from 1.3 to 1.5, with structural parameters of  $T=250\,\mathrm{nm}$  and  $H=300\,\mathrm{nm}$ , and electronic properties of  $E_F=0.64\,\mathrm{eV}$  and  $\mu=10000\,\mathrm{c}\,\mathrm{m}^2/(\mathrm{V.s})$ . The optical absorption spectra of crumpled graphene on silicon substrate for various (c)  $\mu$  from 1000 to 10000 cm²/(V.s) at  $n_1=1.3$  and  $E_F=0.64\,\mathrm{eV}$ , (d)  $n_1$  from 1.3 to 1.5 at  $E_F=0.64\,\mathrm{eV}$  and  $\mu=4000\,\mathrm{c}\,\mathrm{m}^2/(\mathrm{V.s})$ , and (e)  $E_F$  from 0.6 to 0.8 eV at  $n_1=1.3$  and  $\mu=10000\,\mathrm{c}\,\mathrm{m}^2/(\mathrm{V.s})$ . The insets show schematic illustrations of the crumpled graphene placed on the corrugated PDMS film and silicon substrate.

Table 2. Comparison of the sensing performance of the proposed crumpled graphene structure with recently published refractive index sensors in the mid-infrared region.

| Recently published refractive index sensors  | Plasmon resonance<br>Wavelength (µm) | Max sensitivity (µm/RIU) | Max FOM<br>(RIU <sup>-1</sup> ) |
|--|--------------------------------------|--------------------------|---------------------------------|
| few-layer graphene/hBN nanoribbons (2019) [46]   | 6.8                                  | 4.207                    | 57.47                           |
| Graphene Ribbon Arrays (2019) [47]   | 7.5                                  | 2.9                      | 10                              |
| hybrid structure of graphene stripe combined with gold gap-ring (2017) [48]  | 2.3                                  | 1.15                     | 383                             |
| graphene-decorated grating on high dielectric substate (2019) [49]   | 5.5                                  | 2.78                     | 17                              |
| Graphene-based diffractive grating structure (2017) [30]   | 9.5                                  | 2                        | 14.2                            |
| Dual-band graphene metamaterials (2019)<br>[50] graphene-based plasmon induced<br>transparency waveguide (2018) [51] | 7.85 10.1                            | 2.88 4.16                | 12.9 27                         |
| Crumpled graphene sensor supported on silicon substrate with $T = 250$ nm and $H = 300$ nm in this study             | 15.4                                 | 7.49                     | 62.5                            |

to  $1000~\rm cm^2/(V.s)$ . As can be observed in Fig. 4(c), when the mobility decreases from  $10000~\rm to$   $1000~\rm cm^2/(V.s)$  the Q-factor reduces from 67 to 7.5 for the plasmonic mode at the wavelength of 15.4  $\mu$ m. Also, as shown in Fig. 4(d), when the mobility decreases to  $\mu = 4000~\rm cm^2/(V.s)$ , the FOM of the proposed sensor drops to 14 RIU<sup>-1</sup> for the crumpled graphene on the silicon substrate, while the sensitivity remains constant.

It has been shown that the plasmonic Bragg reflector structure formed in graphene waveguide presents high electrical tunability over a wide wavelength range [52]. By introducing a defect into the plasmonic Bragg reflector, a microcavity with a maximum Q-factor of 50 can be obtained for the defect mode. To compare the wavelength tunability of the plasmonic resonances in the proposed crumpled graphene plasmonic sensor to that achieved in the Bragg reflector based structure, we study the electrical tunability of the plasmonic resonances in crumpled graphene by varying the Fermi energy level of graphene. As shown in Fig. 4(e), with increasing  $E_f$  from 0.6 to 0.8 eV the resonance wavelength blue-shifted from ~16 to ~14 µm, which is larger than that achieved in Bragg reflector structure [52].

The Q-factor for the main plasmonic mode of the crumpled graphene structure on the PDMS and silicon substrates in Fig. 4(a) and Fig. 4(b), when  $n_1$ =1.3, are about 71 and 67, respectively, which are higher than that of plasmonic Bragg reflector structure [52]. Also, the sensitivity and FOM of our proposed crumpled 2D materials based plasmonic biosensor are at least three times higher than that achieved by the Bragg reflector structure [30].

In the following, we will investigate a plasmonic device from crumpled graphene-MoS<sub>2</sub> van der Waals heterostructure. The device is identical in structure to the previously discussed pure graphene device (Fig.1a) with the modification that a MoS<sub>2</sub> layer is added atop the graphene layer supported on a PDMS substrate. In this case, we define the period and the height of the crumpled heterostructure as  $T_t = T$  and  $H_t = H_g + t_{MoS_2} + t_{gap}$ , where  $H_g$ ,  $t_{MoS_2}$ , and  $t_{gap}$  are crumpled graphene height, thickness of the MoS<sub>2</sub> layer, and the gap distance between the graphene and MoS<sub>2</sub> layers, respectively.

The optical absorption of crumpled graphene-MoS<sub>2</sub> heterostructure is shown in Fig. 5 for crumpled structure parameters, including  $T_t = 150$  nm,  $H_g = 350$  nm,  $t_{MoS_2} = 0.7$  nm, and  $t_{gap} = 0$  nm, as well as electronic properties of 2D materials, such as  $E_F = 0.64$  eV,  $\tau_{MoS_2} = 0.17$  ps, and different electron concentration in MoS<sub>2</sub> layer  $(n_{2D})$ . For comparison, the absorption spectra of crumpled graphene and crumpled MoS<sub>2</sub> structures are plotted in the figure. We demonstrated

the influence of the 2D electron concentration in the MoS<sub>2</sub> layer on the plasmonic resonances of the crumpled graphene-  $MoS_2$  heterostructure in Fig. 5. As shown in Fig. 5(b), the wavelength of the main resonance peak (~12.84 µm) in the absorption spectra of the free-standing crumpled graphene-MoS<sub>2</sub> heterostructure at the MoS<sub>2</sub> electron concentration  $n_{2D} = 0.1 \times 10^{13}$  c m<sup>-2</sup> closely matches with the wavelength of plasmon peak of the free-standing crumpled graphene structure. There is no absorption peak in the crumpled MoS<sub>2</sub> structure for this electron concentration. Therefore, the effect of this MoS<sub>2</sub> electron concentration is negligible and the major absorption peaks in Fig. 5(b) arise from the plasmonic resonances in the crumpled graphene structure. By increasing the electron concentration to  $n_{2D} = 10 \times 10^{13}$  c m<sup>-2</sup>, plasmon resonance peaks appear in the crumpled MoS<sub>2</sub> and the resonance wavelengths of the plasmon modes in crumpled graphene-MoS<sub>2</sub> heterostructure shift toward shorter wavelengths. As seen in Fig. 5(c), a new hybrid graphene-MoS<sub>2</sub> plasmon mode, which is blue-shifted compared to main crumpled graphene and MoS<sub>2</sub> plasmon modes, arises due to interaction between optical properties of MoS<sub>2</sub> and graphene layers. By Further increasing  $n_{2D}$  to  $25 \times 10^{13}$  c m<sup>-2</sup> (see Figs. 5(d)), the resonance peaks of the MoS<sub>2</sub> plasmon modes, and therefore hybrid graphene-MoS<sub>2</sub> plasmon modes, shift toward shorter wavelengths, become sharper, and the intensity of the absorption peaks increases. The main plasmon mode of the combined graphene-MoS<sub>2</sub> structure creates a slightly sharper resonance peak with an FWHM of 175 nm and with a higher intensity of 0.36 on the normal-incidence absorption spectra compared to that of the crumpled graphene (with FWHM of 195 nm and intensity of 0.3) and crumpled MoS<sub>2</sub> (with FWHM of 224 and intensity 0.26) structures.

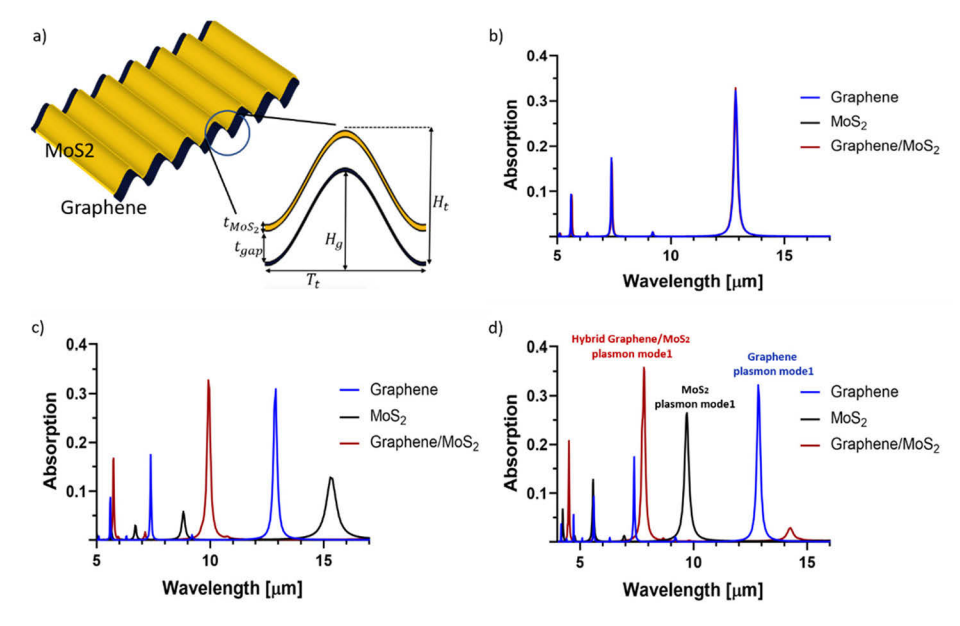


**Fig. 5.** Hybrid plasmonic resonance of crumpled graphene-MoS<sub>2</sub> heterostructure. (a) The schematic illustrations of the free-standing crumpled graphene-MoS<sub>2</sub> heterostructure. optical absorption spectra of free-standing crumpled graphene (blue line), crumpled MoS<sub>2</sub> (black line), and graphene-MoS<sub>2</sub> heterostructure (red line) with structural parameters of  $T_t = 150 \text{ nm}$  and  $H_t = 350 \text{ nm}$ , and carrier concentration of (b)  $n_{2D} = 0.1 \times 10^{13} \text{c m}^{-2}$ , (c)  $n_{2D} = 10 \times 10^{13} \text{c m}^{-2}$ , and (d)  $n_{2D} = 25 \times 10^{13} \text{c m}^{-2}$  in MoS<sub>2</sub> flake. The electronic parameters of graphene flake are set as  $E_F = 0.64 \text{ eV}$  and  $\mu = 10000 \text{c m}^2/(\text{V.s})$ .

As mentioned above (Fig. 2), the graphene plasmon resonances, and therefore the sensitivity of the device is influenced by damping effect due to the high absorbance of PDMS substrate in

the wavelength range from 8to 15 µm. Using the crumpled graphene-MoS<sub>2</sub> heterostructure, the plasmon modes blueshift toward the shorter wavelength resulting in a large detuning between the absorbance peaks of PDMS and plasmon resonance wavelengths. This leads to a resonant peak with higher intensity and lower FWHM, which is essential for biosensing applications and increasing sensitivity. The absorption spectra of the crumpled MoS<sub>2</sub>/SiO<sub>2</sub>/graphene heterostructure on the PDMS substrate in the solutions with different refractive indices are shown in Fig. 6(a). It is assumed that the gap area between the MoS<sub>2</sub> and graphene layers is occupied by a thin film of SiO<sub>2</sub> with a thickness of 3 nm. Compared to the main plasmon resonance of the crumpled graphene on PDMS substrate (at the wavelength of  $\sim 10.7 \,\mu m$  in Fig. 4(a)), an obvious blueshift can be observed for the hybrid plasmon resonance of the crumpled heterostructure by 4.4  $\mu$ m in the solution with  $n_1 = 1.3$ . By changing the refractive index atop the crumpled heterostructure from 1.3 to 1.5 the hybrid mode wavelength redshifts from 6.4 to 6.83 µm exhibiting a sensitivity of 2180 nm/RIU and FOM of 18.2 (FWHM = 120 nm). Compared to the crumpled graphene sensor on the PDMS with a sensitivity of 2090nm/RIU and FOM of 12.2 (FWHM = 170 nm), the crumpled  $MoS_2/SiO_2/graphene$  heterostructure shows better sensing performance.

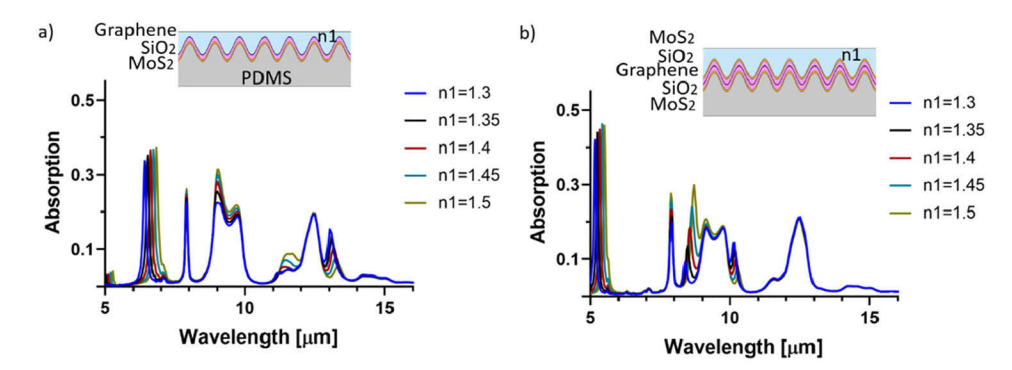


**Fig. 6.** Comparison of plasmonic resonance shifts of crumpled graphene crumpled MoS<sub>2</sub>/SiO<sub>2</sub>/graphene and crumpled MoS<sub>2</sub>/SiO<sub>2</sub>/graphene/SiO<sub>2</sub>/MoS<sub>2</sub> heterostructures. (a) Normal-incidence optical absorption spectra of a crumpled MoS<sub>2</sub>/SiO<sub>2</sub>/graphene, and (b) crumpled MoS<sub>2</sub>/SiO<sub>2</sub>/graphene/SiO<sub>2</sub>/MoS<sub>2</sub> structures supported on corrugated PDMS substrate when the refractive index of solution atop the crumpled surface  $n_1$  changes from 1.3 to 1.5 with a gap size of 3 nm filled by SiO<sub>2</sub> layer between the MoS<sub>2</sub> and graphene flakes at  $E_F = 0.64 \, \text{eV}$ ,  $\mu = 10000 \, \text{cm}^2/(\text{V.s})$ , and  $n_{2D} = 22 \times 10^{13} \, \text{cm}^{-2}$ . The structural parameters are set as  $T_t = 250 \, \text{nm}$  and  $H_t = 306 \, \text{nm}$ . The insets show schematic illustrations of the crumpled graphene structure, crumpled MoS<sub>2</sub>/SiO<sub>2</sub>/graphene, and crumpled MoS<sub>2</sub>/SiO<sub>2</sub>/graphene/SiO<sub>2</sub>/MoS<sub>2</sub> heterostructures placed on the corrugated PDMS substrates.

Further wavelength detuning between the plasmon and PDMS absorbance resonances can be obtained using  $MoS_2/SiO_2/graphene/SiO_2/MoS_2$  heterostructures. As seen in Fig. 6(b), the hybrid plasmon modes of crumpled  $MoS_2/SiO_2/graphene/SiO_2/MoS_2$  blueshift to shorter wavelengths ranging from 5.17 to 5.51  $\mu$ m for all solution samples with different refractive indices between 1.3 to 1.5, compared to that of the crumpled  $MoS_2/SiO_2/graphene$  heterostructure.

Finally, by depositing a thin metallic layer on the silicon substrate, plasmon resonance peaks with higher intensity and lower FWHM can be achieved. This further enhances the detection signal, and slightly improves the sensor sensitivity. As shown in Fig. 7(a), adding a thin Au layer with a thickness of 30 nm on the silicon substrate enhances the intensity of the plasmon resonance of the crumpled MoS<sub>2</sub>/SiO<sub>2</sub>/graphene/SiO<sub>2</sub>/MoS<sub>2</sub> structure at the wavelength of 4.62 µm by a factor of 1.69 and decreases the FWHM down to 50.7 nm. Compared to the silicon

substrate (Fig. 7(b)), the sensor sensitivity is also enhanced by 363.7 nm/RIU for this plasmon mode (Fig. 7(c)).

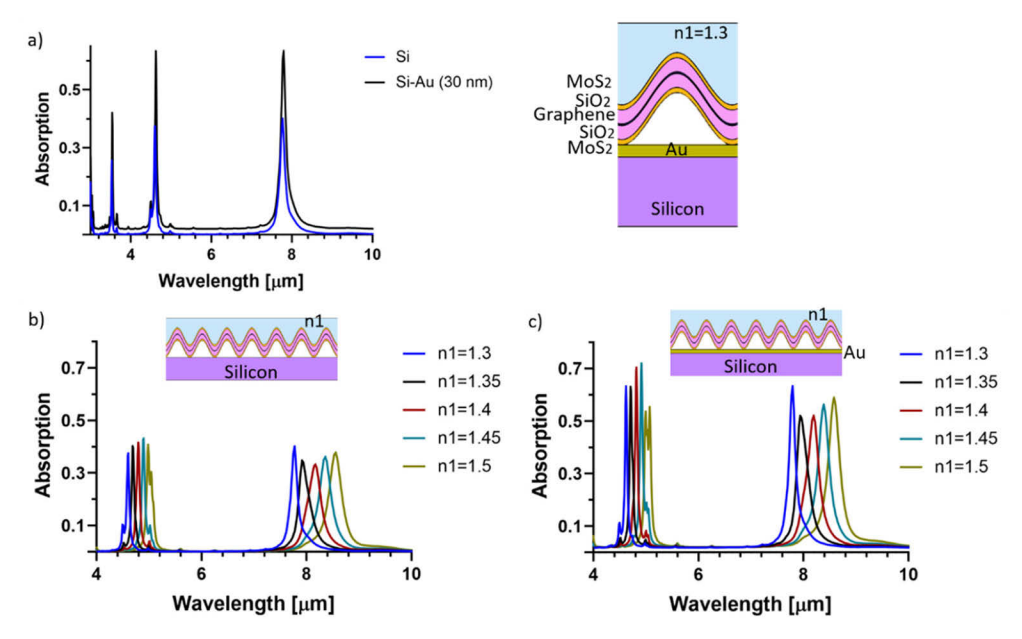


**Fig. 7.** The effect of metallic substrate on plasmonic resonance shifts of crumpled MoS<sub>2</sub>/SiO<sub>2</sub>/graphene/SiO<sub>2</sub>/MoS<sub>2</sub> heterostructures. (a) optical absorption spectra of crumpled MoS<sub>2</sub>/SiO<sub>2</sub>/graphene/SiO<sub>2</sub>/MoS<sub>2</sub>on silicon (blue line) and silicon-Au (black line) substrates in the solution with refractive index n1 = 1.3. A thin film of Au film with a thickness of 30 nm is assumed to deposit on the silicon substrate. The insets show schematic illustrations of the crumpled MoS<sub>2</sub>/SiO<sub>2</sub>/graphene/SiO<sub>2</sub>/MoS<sub>2</sub> supported on the silicon and silicon-Au substrates. (b) optical absorption spectra of crumpled MoS<sub>2</sub>/SiO<sub>2</sub>/graphene/SiO<sub>2</sub>/MoS<sub>2</sub>on silicon substrate when the refractive index of solution atop the MoS<sub>2</sub> surface  $n_1$  changes from 1.3 to 1.5, with structural parameters of  $T_t = 250$  nm and  $H_t = 306$  nm, and electronic properties of  $E_F = 0.64$  eV,  $\mu = 10000$ c m<sup>2</sup>/(V.s), and  $n_{2D} = 22 \times 10^{13}$ c m<sup>-2</sup>. (c) optical absorption spectra of crumpled MoS<sub>2</sub>/SiO<sub>2</sub>/graphene/SiO<sub>2</sub>/MoS<sub>2</sub>supported on Au-silicon substrate with varying the refractive index of solution atop the MoS<sub>2</sub> from 1.3 to 1.5.

It should be noted that the proposed  $MoS_2$ /graphene-based biosensor has the advantages of the facile fabrication process and broadband spectral tunability of strong plasmonic resonances from the mid-to near-infrared by mechanical reconfiguration of crumpled graphene/ $MoS_2$  structures. We have revealed that crumpled graphene/ $MoS_2$  structures are able to be utilized as a refractive index sensor with better performance than conventional graphene-based refractive index sensors. We declare that the main strength of our proposed plasmonic sensor is 3- dimensional (3D) configuration of the crumpled graphene/ $MoS_2$  structure providing more cross-sectional surface area of 2D materials in contact with biomaterials in all directions, especially near the apex and valley regions of the crumpled structure whereas strong local field confinement and enhancements occur. This is the reason for the enhanced sensitivity of crumpled graphene/ $MoS_2$  structures.

In practical biosensing applications, the effect of the stretchable polymer-based substrate may not be easily excluded. As shown above, the PDMS layer possesses high optical absorption in the mid-infrared region which can drastically overlap with surface plasmon resonances. Therefore, in such a strongly interacting system the biomolecular response cannot be isolated because the sensor signal can be overwhelmed by the large optical response of the PDMS layer. This problem can be addressed using crumpled 2D materials heterostructure by shifting the plasmon resonances

outside the destructive absorbance region of PDMS. With a large detuning between the plasmon resonances and PDMS absorbance peaks, distinct spectral peaks and shifts of the plasmon resonances in the presence of biomolecules can be revealed in the crumpled heterostructures with higher sensitivity and larger FOM (narrower spectral width), compared to crumpled graphene structure. In contrast to the strong-coupling regime between the PDMS absorbance and plasmon resonances, one can isolate the distinct plasmon resonances with higher absorbance intensity and lower FWHM by detuning the PDMS absorbance peaks from the plasmon resonances. Another way to avoid the damping effect of PDMS substrate is by transferring crumpled graphene structure onto the transparent substrate in mid-infrared.

It is worth noting that mechanical reconfiguration of crumpled graphene may not be essential for graphene plasmonic biosensors supported on the transparent mid-infrared substrate, as the plasmon resonances of the graphene can be detected over a broad spectral range in mid-infrared using these transparent substrates. Instead, it is highly crucial for graphene sensors placed on the stretchable and flexible polymer-based substrate, such as PDMS, to induce a large detuning between the plasmon resonances and substrate absorbance peaks and avoid damping of plasmonic resonances due to the substrate.

#### 4. Conclusion

In summary, we proposed a high-sensitivity plasmonic biosensor based on the crumpled graphene/MoS<sub>2</sub> structure in which plasmon resonances in crumpled graphene and MoS<sub>2</sub> structures are used to detect small changes in the refractive index of the solution. The novel crumpled configuration enables strong interaction between the sensing medium and plasmonic wave, which enhances the sensitivity of the device by inducing a large shift in resonance wavelength. To avoid damping effect of the PDMS substrate, the crumpled graphene structure can be transferred on the mid-infrared transparent substrate such as silicon by removing the PDMS layer. High sensitivity amounts of up to 7499 nm/RIU has been obtained for the main resonance peaks in crumpled graphene structures supported on silicon substrate corresponding to a FOM of 62.5 RIU<sup>-1</sup>. The sensing properties can be tuned by mechanical reconfiguration of structural parameters over a broad spectral range in the infrared region. Also, using the crumpled MoS<sub>2</sub>-graphene heterostructure the plasmon resonances can be detuned from the PDMS absorbance peaks exhibiting distinct plasmonic resonances with better sensitivity and FOM compared to the crumpled graphene on the PDMS substrate. The enhanced sensitivity along with facile structural turnability are the major advances of our refractive index sensor. Therefore, the proposed crumpled 2D material structure is a promising method for potential applications in designing and developing simple and high-performance biosensing devices based on plasmonic waves.

**Acknowledgments.** This research was partially supported by the NSF through the University of Illinois at Urbana-Champaign Materials Research Science and Engineering Center DMR-1720633. The authors also acknowledge the Iran Nanotechnology Initiative Council (INIC) for partial support of this project.

**Disclosures.** The authors declare no conflicts of interest.

**Data availability.** Data underlying the results presented in this paper are not publicly available at this time but may be obtained from the authors upon reasonable request.

#### References

- 1. S. A. Maier, Plasmonics: Fundamentals and Applications (Springer, 2007).
- V. Kaur and S. Singh, "A dual-channel surface plasmon resonance biosensor based on a photonic crystal fiber for multianalyte sensing," J. Comput. Electron. 18(1), 319–328 (2019).
- Y. Gao, G. Ren, B. Zhu, L. Huang, H. Li, B. Yin, and S. Jian, "Tunable plasmonic filter based on graphene split-ring," Plasmonics 11(1), 291–296 (2016).
- S. Wang, X. Y. Wang, B. Li, H. Z. Chen, Y. L. Wang, L. Dai, R. F. Oulton, and R. M. Ma, "Unusual scaling laws for plasmonic nanolasers beyond the diffraction limit," Nat. Commun. 8(1), 1889 (2017).

- 5. M. Kaboli and M. Akhlaghi, "Investigating the optical AND gate using plasmonic nano-spheres," J. Comput. Electron. **15**(1), 295–300 (2016).
- M. Klein, B. H. Badada, R. Binder, A. Alfrey, M. McKie, M. R. Koehler, D. G. Mandrus, T. Taniguchi, K. Watanabe, B. J. LeRoy, and J. R. Schaibley, "2D semiconductor nonlinear plasmonic modulators," Nat. Commun. 10(1), 3264 (2019).
- M. J. Linman, K. Sugerman, and Q. Cheng, "Detection of low levels of Escherichia coli in fresh spinach by surface plasmon resonance spectroscopy with a TMB-based enzymatic signal enhancement method," Sensors and Actuators B: Chemical 145(2), 613–619 (2010).
- S. Szunerits and R. Boukherroub, "Sensing using localised surface plasmon resonance sensors," Chem. Commun. 48(72), 8999–9010 (2012).
- S. Laing, L. E. Jamieson, K. Faulds, and D. Graham, "Surface-enhanced Raman spectroscopy for in vivo biosensing," Nat. Rev. Chem. 1(8), 0060 (2017).
- J. Homola, "Surface plasmon resonance sensors for detection of chemical and biological species," Chem. Rev. 108(2), 462–493 (2008).
- I. Abdulhalim, M. Zourob, and A. Lakhtakia, "Surface plasmon resonance for biosensing: A mini-review," Electromagnetics 28(3), 214–242 (2008).
- A. G. Samarentsis, A. K. Pantazis, A. Tsortos, J. M. Friedt, and E. Gizeli, "Hybrid sensor device for simultaneous surface plasmon resonance and surface acoustic wave measurements," Sensors 20(21), 6177 (2020).
- Á. I. López-Lorente and B. Mizaikoff, "Mid-infrared spectroscopy for protein analysis: potential and challenges," Anal. Bioanal. Chem. 408(11), 2875–2889 (2016).
- S. Berweger, D. M. Nguyen, E. A. Muller, H. A. Bechtel, T. T. Perkins, and M. B. Raschke, "Nano-chemical infrared imaging of membrane proteins in lipid bilayers," J. Am. Chem. Soc. 135(49), 18292–18295 (2013).
- Y. Zhong, S. D. Malagari, T. Hamilton, and D. Wasserman, "Review of mid-infrared plasmonic materials," J. Nanophotonics 9(1), 093791 (2015).
- B. Fotouhi, V. Ahmadi, and V. Faramarzi, "Nano-plasmonic-based structures for DNA sequencing," Opt. Lett. 41(18), 4229 (2016).
- 17. B. Fotouhi, V. Ahmadi, M. Abasifard, and V. Faramarzi, "Petahertz-frequency plasmons in graphene nanopore and their application to nanoparticle sensing," Scientia Iranica 24(3), 1669–1677 (2017).
- Y. Liu, S. Palomba, Y. Park, T. Zentgraf, X. Yin, and X. Zhang, "Compact magnetic antennas for directional excitation of surface plasmons," Nano Lett. 12(9), 4853–4858 (2012).
- H. J. Li, L. L. Wang, B. Sun, Z. R. Huang, and X. Zhai, "Controlling mid-infrared surface plasmon polaritons in the parallel graphene pair," Appl. Phys. Express 7(12), 125101 (2014).
- V. Faramarzi, V. Ahmadi, B. Fotouhi, and M. Abasifard, "A potential sensing mechanism for DNA nucleobases by optical properties of GO and MoS2 Nanopores," Sci. Rep. 9(1), 6230 (2019).
- 21. A. N. Grigorenko, M. Polini, and K. S. Novoselov, "Graphene plasmonics," Nat. Photonics 6(11), 749-758 (2012).
- 22. F. J. García De Abajo, "Graphene nanophotonics," Science 339(6122), 917–918 (2013).
- 23. Z. Fei, A. S. Rodin, G. O. Andreev, W. Bao, A. S. McLeod, M. Wagner, L. M. Zhang, Z. Zhao, M. Thiemens, G. Dominguez, M. M. Fogler, A. H. Castro Neto, C. N. Lau, F. Keilmann, and D. N. Basov, "Gate-tuning of graphene plasmons revealed by infrared nano-imaging," Nature 486(7405), 82–85 (2012).
- T. Low, A. Chaves, J. D. Caldwell, A. Kumar, N. X. Fang, P. Avouris, T. F. Heinz, F. Guinea, L. Martin-Moreno, and F. Koppens, "Polaritons in layered two-dimensional materials," Nat. Mater. 16(2), 182–194 (2017).
- A. P. Hibbins, E. Hendry, M. J. Lockyear, and J. R. Sambles, "Prism coupling to 'designer' surface plasmons," Opt. Express 16(25), 20441 (2008).
- 26. R. S. Anwar, H. Ning, and L. Mao, "Recent advancements in surface plasmon polaritons-plasmonics in subwavelength structures in microwave and terahertz regimes," Digital Communications and Networks 4(4), 244–257 (2018).
- H. Ditlbacher, N. Galler, D. M. Koller, A. Hohenau, A. Leitner, F. R. Aussenegg, and J. R. Krenn, "Coupling dielectric waveguide modes to surface plasmon polaritons," Opt. Express 16(14), 10455 (2008).
- W. Sun, Q. He, S. Sun, and L. Zhou, "High-efficiency surface plasmon meta-couplers: concept and microwave-regime realizations," Light Sci Appl 5, e16003 (2016).
- H. Yan, T. Low, W. Zhu, Y. Wu, M. Freitag, X. Li, F. Guinea, P. Avouris, and F. Xia, "Damping pathways of mid-infrared plasmons in graphene nanostructures," Nat. Photonics 7(5), 39 (2013).
- V. Faramarzi, V. Ahmadi, F. G. Golmohamadi, and B. Fotouhi, "A biosensor based on plasmonic wave excitation with diffractive grating structure," Scientia Iranica 24(6), 3441–3447 (2017).
- 31. D. Rodrigo, O. Limaj, D. Janner, D. Etezadi, F. J. García De Abajo, V. Pruneri, and H. Altug, "Mid-infrared plasmonic biosensing with graphene," Science **349**(6244), 165–168 (2015).
- 32. P. Kang, K. H. Kim, H. G. Park, and S. W. Nam, "Mechanically reconfigurable architectured graphene for tunable plasmonic resonances," Light Sci Appl 7(1), 17 (2018).
- P. Kang, M. C. Wang, P. M. Knapp, and S. Nam, "Crumpled graphene photodetector with enhanced, strain-tunable, and wavelength-selective photoresponsivity," Adv. Mater. 28(23), 4639–4645 (2016).
- J. Leem, M. C. Wang, P. Kang, and S. Nam, "Mechanically self-assembled, three-dimensional graphene-gold hybrid nanostructures for advanced nanoplasmonic sensors," Nano Lett. 15(11), 7684–7690 (2015).
- A. Krishna, J. M. Kim, J. Leem, M. C. Wang, S. Nam, and J. Lee, "Ultraviolet to mid-infrared emissivity control by mechanically reconfigurable graphene," Nano Lett. 19(8), 5086–5092 (2019).

- 36. M. T. Hwang, M. Heiranian, Y. Kim, S. You, J. Leem, A. Taqieddin, V. Faramarzi, Y. Jing, I. Park, A. M. van der Zande, S. Nam, N. R. Aluru, and R. Bashir, "Ultrasensitive detection of nucleic acids using deformed graphene channel field effect biosensors," Nat. Commun. 11(1), 1543 (2020).
- 37. A. Ganguli, V. Faramarzi, A. Mostafa, M. T. Hwang, S. You, and R. Bashir, "High sensitivity graphene field effect transistor-based detection of DNA amplification," Adv. Funct. Mater. 30(28), 2001031 (2020).
- 38. A. Prasad, A. Chaichi, A. Mahigir, S. P. Sahu, D. Ganta, G. Veronis, and M. R. Gartia, "Ripple mediated surface enhanced Raman spectroscopy on graphene," Carbon 157, 525–536 (2020).
- 39. J. T. Lin, D. C. Cheng, M. Jiang, Y. S. Chiang, and H. W. Liu, "Analysis of scaling law and figure of merit of fiber-based biosensor," *J. Nanomater.* (2012).
- M. S. Hwang, H. R. Kim, K. H. Kim, K. Y. Jeong, J. S. Park, J. H. Choi, J. H. Kang, J. M. Lee, W. Il Park, J. H. Song, M. K. Seo, and H. G. Park, "Switching of photonic crystal lasers by graphene," Nano Lett. 17(3), 1892–1898 (2017).
- W. Gao, J. Shu, C. Qiu, and Q. Xu, "Excitation of plasmonic waves in graphene by guided-mode resonances," ACS Nano 6(9), 7806–7813 (2012).
- V. Y. Reshetnyak, V. I. Zadorozhnii, I. P. Pinkevych, T. J. Bunning, and D. R. Evans, "Surface plasmon absorption in MoS2 and graphene-MoS2 micro-gratings and the impact of a liquid crystal substrate," AIP Advances 8(4), 045024 (2018).
- 43. S. D. Gedney, "Introduction to the finite-difference time-domain (FDTD) method for electromagnetics," Synthesis Lectures on Computational Electromagnetics 27, 1–250 (2011).
- 44. J. Kischkat, S. Peters, B. Gruska, M. Semtsiv, M. Chashnikova, M. Klinkmüller, O. Fedosenko, S. MacHulik, A. Aleksandrova, G. Monastyrskyi, Y. Flores, and W. T. Masselink, "Mid-infrared optical properties of thin films of aluminum oxide, titanium dioxide, silicon dioxide, aluminum nitride, and silicon nitride," Appl. Opt. 51(28), 6789–6798 (2012).
- X. Zhang, J. Qiu, J. Zhao, X. Li, and L. Liu, "Complex refractive indices measurements of polymers in infrared bands," Appl. Opt. 252, 2337 (2020).
- H. Jiang, S. Choudhury, Z. A. Kudyshev, D. Wang, L. J. Prokopeva, P. Xiao, Y. Jiang, and A. V. Kildishev, "Enhancing sensitivity to ambient refractive index with tunable few-layer graphene/hBN nanoribbons," Photonics Res. 7(7), 815 (2019).
- 47. H. Yang, Z. Li, F. Li, H. Liu, C. Teng, H. Deng, R. Xu, S. Deng, and L. Yuan, "High-sensitivity plasmonics biosensor based on graphene ribbon arrays," in 2019 7th International Conference on Information, Communication and Networks, ICICN 2019, 105–108, (2019).
- 48. Z. Du, B. Hu, P. Cyril, J. Liu, and Y. Wang, "High sensitivity plasmonic sensor using hybrid structure of graphene stripe combined with gold gap-ring," Mater. Res. Express 4(10), 17 (2017).
- K. Tong, Y. Wang, F. Wang, J. Sun, and X. Wu, "Surface plasmon resonance biosensor based on graphene and grating excitation," Appl. Opt. 58(7), 1824 (2019).
- S. Gong, B. Xiao, L. Xiao, S. Tong, S. Xiao, and X. Wang, "Hybridization-induced dual-band tunable graphene metamaterials for sensing," Opt. Mater. Express 9(1), 35 (2019).
- D. Wu, J. Tian, L. Li, and R. Yang, "Plasmon induced transparency and refractive index sensing in a new type of graphene-based plasmonic waveguide," Opt. Commun. 412, 41–48 (2018).
- 52. J. Tao, X. Yu, B. Hu, A. Dubrovkin, and Q. J. Wang, "Graphene-based tunable plasmonic Bragg reflector with a broad bandwidth," Opt. Lett. 39(2), 271 (2014).